of CCl_4 in the atmosphere not exceeding 280 parts per 10^{12} and probably lower.

The high concentrations of CCl_4 in Los Angeles, the North Atlantic, the Arctic Ocean, and western Ireland (Fig. 1b) could be due to the regional buildup of CCl_4 over populated areas in favorable meteorological conditions followed by advection of the polluted air to the area where measurements were made. Examination of monthly mean sea-level pressure charts for the time of the Los Angeles and North Atlantic observations indicates that such an interpretation is possible.

It has been suggested that the lifetime of CCl_4 in the atmosphere can be determined from the relative standard deviation of the atmospheric concentration of CCl_4 (*1*, *20*). However, this method is not applicable if the limit of instrument reproducibility for a measurement is comparable with the real variation in atmospheric concentration or if the atmospheric measurements are made in the vicinity of local sources or sinks. On the basis of the loss mechanisms described here, it appears that the atmospheric lifetime of CCl_4 is of the order of several decades.

I. E. GALBALLY
Division of Atmospheric Physics,
Commonwealth Scientific and Industrial
Research Organization, Aspendale,
Victoria, Australia

References and Notes

1. J. E. Lovelock, R. J. Maggs, R. J. Wade, *Nature (London)* **241**, 194 (1973); J. E. Lovelock, *ibid.* **252**, 292 (1974).
2. A. J. Murray and J. P. Riley, *ibid.* **242**, 37 (1973); P. E. Wilkniss, R. A. Lamontagne, R. E. Larson, J. W. Swinnerton, C. R. Dickson, T. Thompson, *ibid.* **245**, 45 (1973); P. G. Simmonds *et al.*, *Atmos. Environ.* **8**, 209 (1974); P. E. Wilkniss, J. W. Swinnerton, D. J. Bressan, R. A. Lamontagne, R. E. Larson, *J. Atmos. Sci.* **32**, 158 (1975); P. L. Hanst, L. L. Spiller, D. M. Watts, J. W. Spence, M. F. Miller, *J. Air Pollut. Control Assoc.* **25**, 1220 (1975); D. H. Pack, in "Geophysical monitoring for climatic change," J. M. Miller, Ed. [Summary Report No. 3 (1974), National Oceanic and Atmospheric Administration, U.S. Department of Commerce, Washington, D.C., 1975], pp. 99–107.
3. M. J. Molina and F. S. Rowland, *Nature (London)* **249**, 810 (1974); *Geophys. Res. Lett.* **1**, 309 (1974); P. Crutzen, *ibid.*, p. 205; R. J. Cicerone, R. S. Stolarski, S. Walters, *Science* **185**, 1165 (1974); S. C. Wofsy, M. B. McElroy, N. D. Sze, *ibid.* **187**, 535 (1975).
4. R. J. Cicerone, D. H. Stedman, R. S. Stolarski, *Geophys. Res. Lett.* **2**, 219 (1975).
5. M. J. Molina and F. S. Rowland, *ibid.* **1**, 309 (1974).
6. F. S. Rowland and M. J. Molina, *Rev. Geophys. Space Phys.* **13**, 1 (1975).
7. R. J. Cicerone, *J. Geophys. Res.* **80**, 3911 (1974).
8. J. E. Lovelock and D. H. Pack, personal communications. Lovelock writes: "It is possible that carbon tetrachloride ultimately can be assigned a human source but it would appear that it is originating via some atmospheric or surface chemical processes from either halocarbons or the other chlorine carrying precursors." The alternative view presented in this report is that CCl_4 is man-made and subsequently released to the atmosphere.
9. P. S. Brallier, in *Kirk-Othmer Encyclopedia of Chemical Technology* (Wiley, New York, ed. 1, 1949), vol. 3, pp. 191–200; D. F. W. Hardie, in *Kirk-Othmer Encyclopedia of Chemical Technology* (Wiley, New York, ed. 2, 1964), vol. 5, pp. 128–139; J. W. Wyart and M. F. Dante, in *ibid.* (ed. 2, 1969), vol. 18, pp. 564–588; R. L. McCarthy, paper presented at the meeting of the American Geophysical Union, San Francisco, 13 December 1974.
10. G. McConnell, D. M. Ferguson, C. R. Pearson, *Endeavour* **34**, 13 (1975).
11. R. L. McCarthy and J. P. Jesson, paper presented at the annual meeting of the American Chemical Society, Philadelphia, 9 April 1975.
12. G. E. H. Reuter, *Elementary Differential Equations and Operators* (Routledge & Kegan Paul, London, 1958).
13. J. E. Lovelock, personal communication. Lovelock observed during the R.V. *Shackleton* cruise in 1971–1972 a decrease in the concentration of CCl_4 from 95 parts per 10^{12} to 70 parts per 10^{12} while the ship was passing through a region where the air was dense with Sahara dust. Visibility was in the range of 3 km, and the air was blowing from the African continent.
14. P. J. Crutzen, *Tellus* **26**, 47 (1974); P. Warneck, *ibid.*, p. 39; M. B. McElroy, S. C. Wofsy, J. E. Penner, J. C. McConnell, *J. Atmos. Sci.* **31**, 287 (1974); H. S. Johnston, *Adv. Environ. Sci. Technol.* **4**, 263 (1974); R. K. M. Jayanty, R. Simonaitis, J. Heicklen, *J. Photochem.* **4**, 203 (1975); A. Y-M. Ung and H. I. Schiff, *Can. J. Chem.* **40**, 486 (1962); V. N. Kondratiev, *Rate Constants of Gas Phase Reactions* (Publication COM-72-10014, National Bureau of Standards, Washington, D.C., 1972). I have estimated the upper limit of the OH + CCl_4 reaction rate from the molecular collision rate and enthalpy change limitations.
15. J. Heicklen, *Adv. Photochem.* **7**, 57 (1969).
16. P. S. Liss and P. G. Slater, *Nature (London)* **247**, 181 (1974).
17. I have obtained the same loss rate with a more complicated model involving air-ocean exchange, and vertical diffusion and destruction within the mixed layer of the ocean. Laboratory measurements [J. Hine, *J. Am. Chem. Soc.* **72**, 2438 (1950)] would indicate a slower rate of CCl_4 destruction by hydrolysis in water at the same *p*H as the oceans. These results indicate the influence of other constituents on CCl_4 destruction in seawater.
18. C. D. Keeling, in *The Chemistry of the Lower Atmosphere*, S. I. Rasool, Ed. (Plenum, New York, 1973), chap. 6.
19. J. E. Lovelock, unpublished data.
20. C. E. Junge [*Tellus* **26**, 477 (1974)] showed that the relative standard deviation of the concentration of an atmospheric constituent is related to its atmospheric residence time.
21. I thank N. E. Bacon for doing the model computations; I thank Dr. M. F. R. Mulcahy, Dr. J. E. Lovelock, and an anonymous referee for providing helpful comments.

1 December 1975; revised 16 March 1976

Volcanic Dust in Deep-Sea Sediments: Relationship of Microfeatures to Explosivity Estimates

Abstract. *Particle size variations in a series of volcanic ash layers, deposited in high latitudes of the South Pacific during the past 2.5 million years, were earlier analyzed by using a model in which source cloud height and minimum volcanic paleoexplosivity are derived from downwind ash distribution. Examination of submicrometer morphological features of the volcanic glass shards reveals a clear relationship between what appear to be impact features on the glass surfaces and the independently derived paleoexplosivities, which suggests that this may be a simple means to characterize ash horizons and estimate relative volcanic explosivities.*

Atmospherically transported volcanic glass in deep-sea sediments can be readily divided morphologically into categories representing highly explosive or relatively passive eruptions (*1–3*). With increasing distance downwind from a source, rhyolitic glass dust becomes the dominant volcanic constituent, reflecting the high explosivity involved in its production (*1*). Lisitzin (*4*) proposed that such volcanic glass makes up 99 percent of all atmospherically transported volcanic material at distances beyond 1000 km from the source. Megascopically distinguishable ash layers are very rarely found in deep-sea sediments beyond that distance.

We have developed a technique (*5*) for separating and counting fine volcanic glass in deep-sea sediments. By using conventional methods to measure ages and sedimentation rates of the host sediments, the apparent accumulation rate of such glass can then be computed in units of milligrams per 1000 years per square centimeter. Figure 1a shows our published results (*1*) for core E27-3, obtained east of the Balleny Islands (Fig. 1b, inset). We have shown that many of the ash horizons in E27-3 can be recognized in a series of six cores forming a 4000-km traverse east from the islands (*1*, *6*) and have used the observed downwind ash distribution to compute associated volcanic cloud heights, from which paleoexplosivities can be estimated in units of megatons of TNT equivalent (*7*, *8*). The published explosivities for the eruptions indicated in Fig. 1a are all minimum estimates (*9*) and range from 0.1 to 30.0 megatons of TNT equivalent (*10*). The results form the upper scale of Fig. 1b. Because of several ambiguities (such as the assumed net paleowind velocity limits and assumed simple variation of particle size with height in the volcanic cloud), the application of our data (*1*) to the explosivity model (*7*) is somewhat tenuous, and it is therefore desirable to derive independent means to check at least the relative explosivities computed. In this report we consider the merits of microfeature analysis for the resolution of this problem, since there is evidence linking microfeature character and impact velocity in certain natural glasses, particularly in lunar material (*11–17*).

We have noticed that volcanic glass of rhyolitic composition deposited in many deep-sea sediments is characterized morphologically by smooth surfaces when examined with petrographic microscopes (*2*). The higher magnifications obtained with a scanning electron microscope (SEM) reveal, however, a great variety of fine features, including pits, mounds, striations, broken blocks, cracks, and depressions. Submicrometer pits (Fig. 2) are often dominant features, except on vesicular basaltic glass and pumice fragments, where such features are generally absent. Vitreous basaltic flat glass or sideromelane fragments are usually characterized by rough or microvesicular surfaces (*3*), with or without pits. Solution and recrystallization features on deep-sea basaltic glass shards are common, with recrystallization usually occurring along cracks or fractures (*18*). Examination of more than 500 rhyolitic shards derived from a source in the vicinity of the Balleny Islands shows that 92 percent of the pits are between 0.2 and 1.0 μm in diameter, the upper limit being about 10 μm. The morphological types of pits are (i) conchoidal to subconchoidal (Fig. 2, a and d), (ii) elongate (Fig. 2b), (iii) grazing or striated (Fig. 2c), (iv) spherical to ovoidal (Fig. 2d), (v) irregular, and (vi) composite. Most pits are subconcoidal and are randomly distributed on the glass surface (Fig. 2a). The elongate pits are usually oriented in one direction along with elongate mounds embedded in the glass surface (Fig. 2b). The embedded mounds are not common and may be of either glassy substances, the composition apparently being similar to substrate (Fig. 2b), or metallic oxides, as indicated by the isometric crystal form (Fig. 2d). The rare larger pit (up to 10 μm) is usually composite, sometimes occurring as a large central pit with many superimposed submicrometer pits. The center portion of some composite pits exhibits a weblike texture (*11*).

Because of their common occurrence, we have counted the numbers of submicrometer pits (exclusive of other features) per unit area on up to 20 rhyolitic glass shards in the size fraction 61 to 88 μm from each of the eruptions (A1 to G3) shown in Fig. 1a. The pit counts were mostly made by using SEM television images, but many were checked with photomicrographs, particularly when >50 pits per 100 μm^2 were observed. The variance of the pit population for different images of the same shard ranges from ±0.4 to ±5.8 percent, and appears to increase with decreasing pit population. The variance of the pit population between shards in the same eruption is from ±1.6 to ±7.6 percent.

The results for core E27-3 show that the mean pit populations vary from 7 to 126 per 100 μm^2 (Fig. 1b). An important check on the data is provided by examination of shards from the same ash horizons in core E11-9, which was obtained about 3200 km east of E27-3 (Fig. 1b, inset) and which we previously used to demonstrate our capability of detecting ash at large distances from the source (*6*). Evidence of eruptions C1 and C2 was found, on the basis of several criteria, in both E27-3 and E11-9. The results of our pit counts for the ash in E11-9 (Fig. 1b) confirm that the same ash is

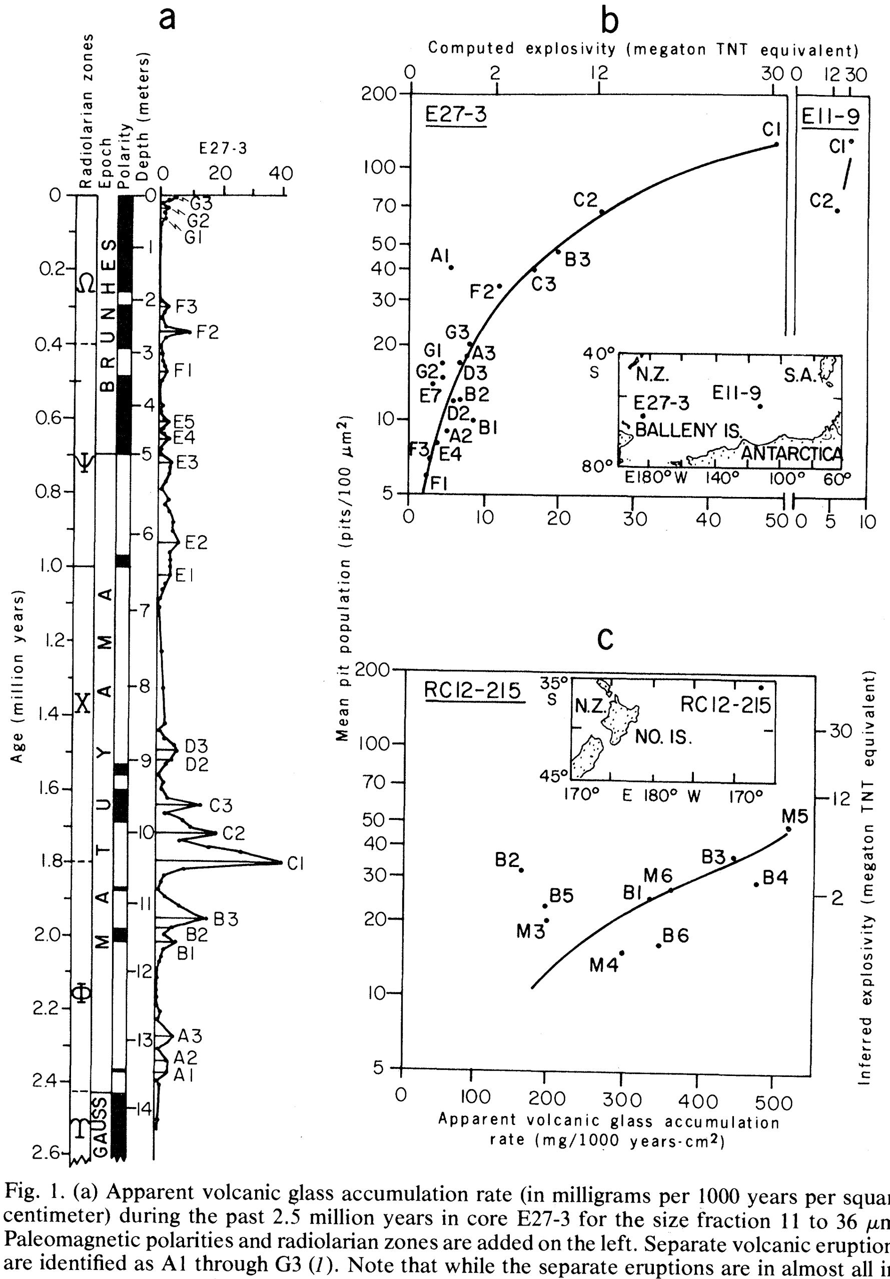

Fig. 1. (a) Apparent volcanic glass accumulation rate (in milligrams per 1000 years per square centimeter) during the past 2.5 million years in core E27-3 for the size fraction 11 to 36 μm. Paleomagnetic polarities and radiolarian zones are added on the left. Separate volcanic eruptions are identified as A1 through G3 (*1*). Note that while the separate eruptions are in almost all instances expressed as simple peaks in the volcanic glass accumulation rate curve, some eruptions such as B2 and D2 are not expressed as discrete peaks in core E27-3. These eruptions are clearly identified, however, in other cores along the 400-km traverse. (b) Mean pit population on volcanic glass shard surfaces, as derived from SEM examination, plotted against apparent volcanic glass accumulation rates for the size fraction 11 to 88 μm in 19 separate eruptions recorded in core E27-3 (a). Paleoexplosivities are based on computations (*10*) for 11 separate eruptions, using the downwind decrease in apparent volcanic glass accumulation rate across six separate cores (*1, 7*). Data for core E11-9 are added on the right (note the scale difference in accumulation rate, which is also for the fraction 11 to 88 μm): eruptions C1 and C2, previously interpreted to correlate with C1 and C2 in E27-3 (*6*), have virtually identical numbers of pits per 100 μm^2 on the volcanic glass surfaces. (Inset) Location of the two cores analyzed: *N.Z.*, New Zealand; *S.A.*, South America. (c) Mean pit population on volcanic glass shard surfaces, as derived from SEM examination, plotted against apparent volcanic glass accumulation rate for the fraction 11 to 88 μm in a series of volcanic ashes east of North Island (*No. Is.*), New Zealand. Core RC12-215, the location of which is shown in the inset, is about 1400 km east of the suspected source region. Approximate ages of eruptions M3 through B6 are about 1.15 to 0.01 million years (*19*). No independently derived paleoexplosivity estimates have yet been computed for the series of eruptions.

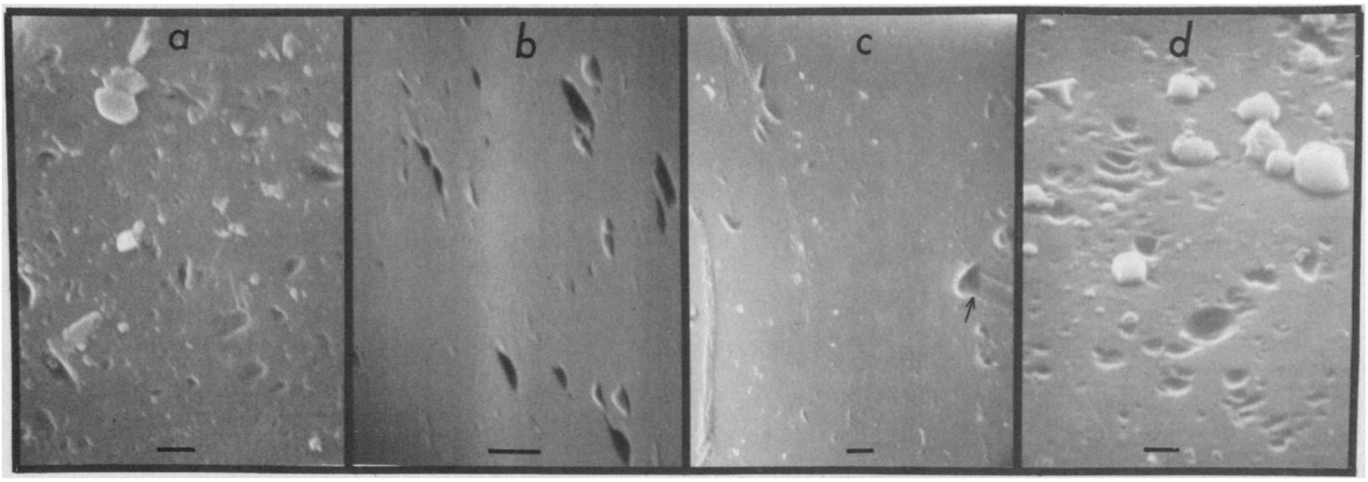

Fig. 2. Photomicrographs of various submicrometer pits and mounds on the deep-sea volcanic glass surfaces. The size fraction used is 61 to 88 μm unless otherwise stated. (a) Flat rhyolitic glass shards in ash layer C2 of core E27-3 (Fig. 1, a and b), showing randomly distributed subconchoidal to irregular pits. (b) Shards in ash layer B2 of core RC12-215 (Fig. 1c), showing elongate pits and embedded elongate silicate mounds. Note that the elongation of all features is undirectional. (c) Shards in ash layer F1 of core E27-3 (Fig. 1, a and b), showing striated or grazing pits. Note (arrow) one pit with possible impact direction feature. (d) Shards of the size fraction 43 to 61 μm in ash layer B3 of core RC12-215, showing conchoidal to spherical and close-spaced multiple pits. Mounds are probably isometric crystals of metallic oxide. Scale bar = 1 μm.

present in both cores, since the number of pits per 100 μm^2 is virtually identical. Therefore, in principle, the pit population can be utilized as a factor in correlation of deep-sea ashes although, as Fig. 1b shows, no simple distinction emerges between the eruptions of lower explosivity. Polynomial regression analysis between the volcanic glass accumulation rates and the mean pit populations in E27-3 shows a significant linear correlation (r^2 = 93.24 percent) between PP (the mean pit population in pits per 100 μm^2) and GAR (the apparent volcanic glass accumulation rate in milligrams per 1000 years per square centimeter), yielding the equation

$$PP = 1.10 + 2.55\,GAR \qquad (1)$$

Electron probe analysis of the shards for different eruptions reveals little range in the major element chemistry of the ashes between eruptions, so that Eq. 1 is not reflecting any simple chemical differences between eruptions. If the paleoexplosivities (W, in megatons of TNT equivalent) computed (*1*, *10*) for the separate eruptions by examination of the downwind decrease in GAR in the traverse of cores are compared to the PP values derived for core E27-3, we find a second linear relation

$$W = 0.25\,PP - 4.38 \qquad (2)$$

For this relation r^2 = 92.91 percent, which leaves only about 7 percent of the relation between W and PP unaccounted for by the regression. Since W results from totally independent analyses of ash from six separate cores up to 4000 km from the source (*1*, *10*) and there is a systematic decrease of more than an order of magnitude in GAR across the traverse, we interpret Eq. 2 as showing that W and PP are closely related. This indicates that at least the relative values of the initial paleoexplosivity estimates (*1*) for the eruptions recorded in E27-3 are acceptable and that our model for the analysis of downwind distributions of ash (*7*) is sound for this series of eruptions in this region.

A similar analysis of a series of ash layers in core RC12-215, east of North Island, New Zealand (Fig. 1c, inset), yields (*19*)

$$PP = 1.18 + 0.08\,GAR \qquad (3)$$

Application of Eq. 2 to the data in core RC12-215 provides estimates of W ranging from 0.1 to 7.6 megatons of TNT equivalent (*19*), but it is not yet possible to test this result because there is no core traverse suitably oriented for measuring the downwind decrease in GAR. The refractive indices of the rhyolitic ashes in the two areas (Fig. 1, b and c) are 1.496 to 1.508 for E27-3 and E11-9 and 1.498 to 1.500 for RC12-215, which shows that the SiO_2 compositions are virtually the same; this would be a minimum requirement for the application of Eq. 2 to eruptions other than those recorded in cores E27-3 and E11-9.

Our analysis has revealed a strong apparent dependence of pit population on volcanic explosivity, and so it is appropriate to speculate on the origin of the pits. The morphology of the pits does not suggest association with a degassing process, because none of the craters show any evidence of collapse on the outer rims, as usually found on vesicles (*2*, *3*). Instead, they more closely resemble lunar impact microcraters (*12–16*) formed under perpendicular, oblique, and grazing impacts (*20*). The absence of fracture and spall zones and glass-lined features, commonly found on lunar microcraters, may indicate lower-velocity impacts (*14*, *21*), which might be expected where impacts result from velocity differences in a volcanic gas column moving at about 600 m/sec (*22–25*). Cracks and broken block microfeatures occur only in shards from eruptions with computed explosivities >20 megatons of TNT equivalent, and submicrometer silicate and metal oxide fragments are occasionally found embedded in the glass surfaces (Fig. 2, b and d). While we are as yet unable to be definitive about the origin of the pits, we can state with confidence that the number of pits per unit area is a strong function of the volcanic explosivity, derived from the downwind distribution of the ash across the high latitudes of the South Pacific, and that microfeature analysis of glass shards is therefore a promising means for understanding at least the relative magnitudes of explosivities in ancient volcanic eruptions.

T. C. HUANG, N. D. WATKINS

Graduate School of Oceanography,
University of Rhode Island,
Kingston 02881

References and Notes

1. T. C. Huang, N. D. Watkins, D. M. Shaw, *Geol. Soc. Am. Bull.* **86**, 1305 (1975).
2. G. Heiken, *ibid.* **83**, 1961 (1972).
3. ———, *Smithson. Contrib. Earth Sci.* *12* (1974).
4. A. P. Lisitzin, *Soc. Econ. Paleontol. Mineral. Spec. Publ.* *17* (1972).
5. T. C. Huang, N.D. Watkins, D. M. Shaw, *Deep-Sea Res.* **22**, 185 (1975).
6. → ———, J. P. Kennett, *Earth Planet. Sci. Lett.* **20**, 119 (1973).
7. D. M. Shaw, N. D. Watkins, T. C. Huang, *J. Geophys. Res.* **79**, 3057 (1974).
8. Hitherto, the term explosivity, when associated

with volcanic eruptions, has generally been confined to such factors as the ratio of pyroclastics to effusive products for a particular eruption [for example, see A. Rittman, *Volcanoes and Their Activity* (Interscience, New York, 1962)]. While clearly logical, such a definition should not prevent use of the term when different techniques and concepts are developed to study the same phenomenon. Our model is designed to measure volcanic cloud heights, and we prefer to use a simple transformation of the result into the equivalent explosive energy needed to create such a cloud (*7*).

9. After the cloud height is computed using methods described in Shaw *et al.* (*7*), the equation of B. R. Morton, G. Taylor, and J. S. Turner [*Proc. R. Soc. London Ser. A* **234**, 23 (1956)] can be applied to derive explosive energy in joules. The result can then be expressed in megatons of TNT equivalent, where 1 megaton = 3.4×10^{15} joules. We stress here that the equation of Morton *et al.* relating cloud height and explosivity can be one of two types, depending on whether the explosion is assumed to be instantaneous or of long duration. The latter assumption results in explosivity estimates up to two orders of magnitude higher. In our analyses we assume instantaneous explosions, and therefore obtain minimum estimates of the energy released to form volcanic clouds at the independently computed heights.
10. The between-core downwind decrease in the volcanic glass accumulation rate for the series of eruptions (Fig. 1a) was used to compute, by exponential extrapolation, the distance at which the rate reaches zero (the maximum distance traveled by the ash). This was done for each separate volcanic dust layer, using the mean for each of three separate particle size ranges: 45 to 36, 35 to 29, and 28 to 23 μm. The apparent cloud height was then derived for each particle size, using equations summarized graphically in figures 5 and 7 of Shaw *et al.* (*7*), and the results were averaged before application of the equation of Morton *et al.* (*9*) relating cloud height to explosivity. Eleven eruptions (*1*, table 4) were amenable to this analysis (eruptions B1, B2, B3, C1, C2, C3, D2, D3, E5, F2, and F3 in Fig. 1a of this report).
11. J. L. Carter, H. C. J. Taylor, E. Padovani, *EOS* **54**, 582 (1973).
12. A. F. Hörz, J. B. Hartung, D. E. Gault, *J. Geophys. Res.* **76**, 5770 (1971).
13. J. F. Vedder, *Earth Planet Sci. Lett.* **11**, 291 (1971).
14. J. L. Carter, in *Proceedings of the Second Lunar Science Conference*, A. A. Levinson, Ed. (MIT Press, Cambridge, Mass., 1971), vol. 1, pp. 873–892.
15. J. B. Hartung, F. Hörz, D. E. Gault, in "Proceedings of the third lunar science conference," *Geochim. Cosmochim. Acta* **3**, 2735 (1972).
16. D. E. Brownlee, F. Hörz, J. F. Vedder, D. E. Gault, J. B. Hartung, in "Proceedings of the fourth lunar science conference," *Geochim. Cosmochim. Acta* **3**, 3191 (1973).
17. Attempts have been made to associate the glass crust fraction in intratelluric phenocrysts of airborne ash with eruptive violence by J. D. Meyer [*Bull. Volcanol.* **35**, 358 (1972)] but such an approach can only be used with coarse products close to the volcanic vent.
18. Microfeature analyses of volcanic glass from nonmarine deposits on the island of São Miguel, Azores, also show submicrometer pits, and so their origin cannot be related to abyssal solution effects.
19. N. D. Watkins and T. C. Huang, *N.Z. J. Geol. Geophys.*, in press.
20. D. C. Anderson, B. E. Cunningham, R. G. Dahms, R. G. Morgan, in *Proceedings of the Second Lunar Science Conference*, A. A. Levinson, Ed. (MIT Press, Cambridge, Mass., 1971), vol. 3, pp. 2733–2765.
21. E. C. T. Chao, in "Proceedings of the fifth lunar science conference," *Geochim. Cosmochim. Acta* **1**, 35 (1974).
22. G. P. L. Walker, L. Wilson, E. L. G. Bowell, *Geophys. J. R. Astron. Soc.* **22**, 377 (1971).
23. L. Wilson, *ibid.* **30**, 381 (1972).
24. E. A. Blackburn, L. Wilson, R. S. J. Sparks, *J. Geol. Soc. London*, in press.
25. R. F. Fudali and W. G. Melson, *Bull. Volcanol.* **35**, 383 (1972).
26. Supported by NSF grant DES74-22347. The SEM facility at the Graduate School of Oceanography of the University of Rhode Island is supported by NSF grant DES74-19370 A01 to J. P. Kennett. The electron probe analyses were made by J. W. Pierce of the Smithsonian Institution, Washington, D.C.

29 March 1976; revised 19 May 1976

Sebertia acuminata: A Hyperaccumulator of Nickel from New Caledonia

Abstract. Sebertia acuminata *(Sapotaceae) from New Caledonia has been shown to be a hyperaccumulator of nickel. The nickel content of the latex (25.74 percent on a dry weight basis) is easily the highest nickel concentration ever found in living material. The nickel is in the form of a low-molecular-weight, water-soluble organic complex.*

In recent years a number of plant species have been discovered which have very high concentrations of nickel (*1–5*). Species containing over 1000 μg (0.1 percent) of this element per gram (dry weight basis) have been termed hyperaccumulators (*5*). The unusual aspect of these accumulators is that with the exception of *Hybanthus floribundus* from Western Australia (*2*) and *Alyssum bertolonii* from Italy (*1*) the species discovered so far are confined exclusively to New Caledonia and are mainly of the genera *Homalium* and *Hybanthus* (see Table 1).

The existence of these accumulators has caused considerable interest in the fields of mineral exploration and plant physiology because of the possible association of these plants with nickel mineralization and because of the interesting problems in plant physiology posed by such high accumulations of an element normally toxic to plants.

We have recently discovered the unusually high nickel-accumulating ability of *Sebertia acuminata* Pierre ex Baill. (Sapotaceae). This species is a tree which reaches 10 m in height. It is well known in New Caledonia from the blue-green color of its latex and is therefore known locally as Sève bleue (blue sap). *Sebertia acuminata* is endemic to New Caledonia, is relatively rare, and has never been recorded away from ultrabasic substrates. It is found mainly in the Grand Massif du Sud and in the Tiebaghi Massif in the north of the island, is found more often in forested areas over peridotitic alluvia or colluvia relatively rich in nickel. A typical soil would contain (in approximate percentages) nickel, 0.85;

Table 1. Nickel concentrations in *Sebertia acuminata* compared with values for other hyperaccumulators.

Species	Organ	Locality	Conc. of nickel (percent dry weight)	References
Sebertia acuminata	Latex	New Caledonia	25.74 (11.20*)	This report
	Leaves		1.17	
	Trunk bark		2.45	
	Twig bark		1.12	
	Fruits		0.30	
	Wood		0.17	
Hybanthus floribundus	Leaves	Western Australia	0.71	(*2, 6*)
	Stems		0.26	
	Wood		0.15	
	Fruits		0.13	
	Flowers		0.48	
	Trunk bark		0.17	
Alyssum bertolonii	Leaves	Italy	0.80	(*1*)
Homalium austrocaledonicum	Leaves	New Caledonia	0.18	(*5*)
H. deplanchei	Leaves	New Caledonia	0.19	(*5*)
H. francii	Leaves	New Caledonia	1.45	(*5*)
H. guillainii	Leaves	New Caledonia	0.69	(*3, 5*)
H. kanaliense	Leaves	New Caledonia	0.94	(*4, 5*)
H. mathieuanum	Leaves	New Caledonia	0.17	(*5*)
H. rubrocostatum	Leaves	New Caledonia	0.12	(*5*)
Hybanthus austrocaledonicus	Leaves	New Caledonia	1.38	(*3–5*)
H. caledonicus	Leaves	New Caledonia	0.60	(*3–5*)
Psychotria douarrei	Leaves	New Caledonia	3.40	(*3*)
	Fruits		2.30	
	Trunk bark		5.24	
	Twig bark		5.52	
	Flowers		2.40	
	Wood		0.23	

*Value expressed on wet weight basis.